



Ultrafast room-temperature synthesis of hierarchically porous metal–organic frameworks by a versatile cooperative template strategy

Chongxiong Duan¹ , Jinhao Huo¹ , Feier Li¹ , Minhui Yang¹ , and Hongxia Xi^{1,2,*}

¹ School of Chemistry and Chemical Engineering, South China University of Technology, Guangzhou 510640, People's Republic of China

² Guangdong Provincial Key Laboratory of Atmospheric Environment and Pollution Control, South China University of Technology, Guangzhou Higher Education Mega Centre, Guangzhou 510006, People's Republic of China

Received: 6 June 2018

Accepted: 10 August 2018

Published online:

27 August 2018

© Springer Science+Business Media, LLC, part of Springer Nature 2018

ABSTRACT

Hierarchically porous MOFs (HP-MOFs) are commonly prepared by means of hydrothermal synthesis. Nonetheless, its relatively long crystallization time and harsh synthesis conditions have strongly obstructed the enhancement of HP-MOFs space–time yields (STYs) and the decrease in energy consumption. Herein, a simple and versatile method for preparing various HP-MOFs at room temperature was demonstrated, which had introduced surfactant as the template, whereas zinc oxide (ZnO) has been used as an accelerant. The resulting HP-MOFs showed multimodal hierarchical porous structures and excellent thermal stability. More importantly, the synthesis time was reduced dramatically to 11 min, with a maximal HP-MOFs STY of as high as $2575 \text{ kg m}^{-3} \text{ d}^{-1}$. Furthermore, the rapid formation process of HP-MOFs was examined through quantum chemistry calculation, and a feasible synthesis mechanism was also proposed. Notably, our synthesis strategy had shown a versatility, since other surfactants could also be used as the templates for the rapid room-temperature fabrication of diverse stable HP-MOFs. Importantly, the porosity of the HP-MOFs could be readily tuned through controlling the type of template. Moreover, gas adsorption measurement of HP-MOFs revealed high CH_4 uptake capacity at 298 K due to the increase in surface area and pore volume. Our findings suggest that such method is applicable for the rapid synthesis of a wide variety of HP-MOFs on an industrial scale.

Address correspondence to E-mail: cehxxi@scut.edu.cn

Introduction

Metal–organic frameworks (MOFs), self-assembled from metal ions (or metal clusters) and organic ligands, have attracted considerable attention during the last two decades owing to their fascinating physical and chemical properties, such as high specific surface areas, tunable structures and porosities, as well as designable functionality [1]. Therefore, MOFs, which serve as the functional materials, have exhibited huge potential applications in diverse areas [2, 3], including gas storage [4], adsorption/separation [5], supercapacitor [6], drug delivery [7], sensing [8] and catalysis [9]. Notably, porosity is an essential feature in MOFs, which plays a vital role in functionalization like the diffusion and mass transfer of substrates/products [10, 11]. However, the pore sizes of the majority of MOFs have been reported to be within a micropore range (pore size < 2 nm) during the last few decades [4, 12, 13]. Consequently, the primary application of MOFs has focused on small molecules, which has prevented the large molecules to approach or leave the interior active sites owing to the confinement of pore size [14].

In recent years, tremendous efforts have been dedicated to develop efficient methods to synthesize hierarchically porous MOFs (HP-MOFs) containing micropores and mesopores (or micropores, mesopores and macropores) [15]. Specifically, the increased length of the bridging ligands is an apparent approach to obtain large pores in the resulting MOFs [16]. However, it is inevitably associated with certain difficulties, such as extended ligands synthesis, smaller mesopore size (< 10 nm), reduced porosity, interpenetration, disintegration and instability of crystal frameworks [17, 18]. On the other hand, HP-MOFs can also be synthesized through introducing mesopores and/or macropores into the structures of MOFs via the template strategy [19, 20] and post-synthetic modification [21]. Besides, a couple of new methods are also available, such as ionic liquids assisted synthesis [22], modulator-induced-defect-formation [23] and a spray-drying technology [24]. Typically, HP-MOFs synthesized by these methods are characterized by the superiorities of tunable mesoporosity and abundant active sites [25]. However, these approaches mostly require harsh experimental conditions and tedious downstream treatments (such as a long reaction time at high temperature and pressure and/or special

apparatus) [26, 27], which is energy-consuming and may lead to pollution, a risk of explosion and a low production rate [28–30]. For instance, the space–time yields (STYs, $\text{kg m}^{-3} \text{d}^{-1}$) are usually below $300 \text{ kg m}^{-3} \text{d}^{-1}$ for products synthesized within several hours [28].

Recently, Huo groups reported the room-temperature synthesis of HP-MOFs (HKUST-1) with a high STY ($2035 \text{ kg m}^{-3} \text{d}^{-1}$) by controlling either the synthesis time or the copper source, for the first time [31]. However, it remains challenging to extend this method to prepare other HP-MOFs under facile synthesis conditions [12]. In our previous work, two HP-MOFs including HKUST-1 and ZIF-8 had been successfully prepared under facile synthesis conditions using a modified template strategy [32]. Nevertheless, several key problems have not been solved yet. For instance, (1) the type of surfactants and the produced HP-MOFs are limited; (2) the synthesis time (30 min) is still relatively long, and the STYs ($1123 \text{ kg m}^{-3} \text{d}^{-1}$) are still relatively low for the production of commercially available HP-MOFs; (3) the mechanism of the rapid room-temperature preparation of HP-MOFs has not been illustrated; and (4) the application of H-MOFs has not been explored. To our delight, the synthesis time had been shortened to 11 min after optimizing the synthesis procedure. More strikingly, the resulting HP-MOFs exhibited multimodal hierarchical structures with micropores, mesopores and macropores, together with excellent thermal stability. Notably, the STY of HP-MOFs was up to $2575 \text{ kg m}^{-3} \text{d}^{-1}$, which is much higher than previously reported ($1123 \text{ kg m}^{-3} \text{d}^{-1}$) due to the reduction in synthesis time. In addition, the mechanism of the rapid synthesis of HP-MOFs had been elaborated by means of quantum chemistry (QC) calculations at the molecular level. As anticipated, the introduced amine surfactant could form the template micelles through self-assembly, as well as the addition of zinc oxide (ZnO) and metal ions to form a hydroxy double salt (HDS) intermediate, which could drive the fast growth of MOF crystals. In addition, four other surfactants could also be utilized as templates to rapidly synthesize HP-MOFs. Importantly, this strategy could also be generalized to rapidly synthesize other HP-MOFs, such as hierarchically porous ZIF-8 and ZIF-61. The resultant HP-MOFs showed enhanced CH_4 uptake capacity in comparison with the microporous MOFs.

Experimental

Rapid room-temperature synthesis of hierarchically porous Cu-BTC

All chemicals were commercially available and used as received without further treatment. The HP-MOFs were synthesized with previously reported approaches with only a minor amend [32, 33]; 0.293 g of zinc oxide (ZnO) powder was dispersed in 18 mL N,N -dimethylmethanamide (DMF) and 8 mL deionized water (H_2O) to form nanoslurry through using sonication for 30 min (denoted as solution A). 7.2 mmol of copper nitrate trihydrate ($\text{Cu}(\text{NO}_3)_2 \cdot 3\text{H}_2\text{O}$) was added to 18 mL of H_2O (denoted as solution B), and then, the solution B was added to solution A under fast magnetic stirring to form (Zn, Cu) hydroxy double salt (HDS) (denoted as solution C). Then, 1.0 mL of surfactant (N,N -dimethyloctadecylamine, DOE) and 4 mmol of 1, 3, 5-benzenetricarboxylic acid (H_3BTC) were added to 16 mL of methanol (denoted as solution D). After stirring for 30 min, solution C was added to solution D under fast magnetic stirring for 1 min, and then stand 10 min. After that, the glaucous solid product was collected by filtered. To remove the guest molecules such as surfactant, the solid product was immersed in ethanol at 60 °C with a total duration of 48 h (four times), and then dried overnight in a vacuum oven at 120 °C. The resulting product is denoted as HP-Cu-BTC. Similarly, HP-MOFs synthesized using other surfactants as templates are named as HP-Cu-BTC_X (X = B, C, D and E, where X represents the type of surfactants, B: hexadecyldimethylamine; C: N,N -dimethyltetradecylamine; D: *n*-butyl alcohol; and E: lauric acid). For comparison, conventional Cu-BTC was synthesized by using a solvothermal method following previous report [34], and labeled as C-Cu-BTC.

Rapid room-temperature synthesis of hierarchically porous ZIF-8

(Zn, Zn) HDS was prepared at room temperature and pressure using previously reported method [32, 35]. Specially, 0.406 g of ZnO was dispersed in 10 mL of H_2O (denoted as solution A), and 1.098 g of zinc acetate dihydrate ($\text{Zn}(\text{CH}_3\text{CO}_2)_2 \cdot 2\text{H}_2\text{O}$) was dissolved in 5 mL DMF (denoted as solution B). Mixed up these two solutions and stirred for 24 h, the generation of gel-like viscous fluid indicates the

formation of (Zn, Zn) HDS. Next, 0.493 g of 2-methylimidazole (2Im) and 1.0 mL of DOE were dispersed in 9 mL DMF (denoted as solution C). 3 mL of (Zn, Zn) HDS suspension was added to solution C under magnetic stirring for 1 min, and then stand 10 min. After that, the obtained product was immediately filtered, activated and dried at 120 °C for overnight. The resulting product is denoted as HP-ZIF-8.

Rapid room-temperature synthesis of hierarchically porous ZIF-61

Similar to the above experiment procedures; 0.222 g of 2Im and 0.275 g of imidazole (Im) were dissolved in 10 mL methanol under fast magnetic stirring (denoted as solution A), and 1.0 mL of DOE was added to solution A. After stirring for 30 min, 3 mL of (Zn, Zn) HDS suspension was added to solution A under magnetic stirring for 1 min, and then stand 10 min, then immediately filtered, activated and dried overnight at 120 °C. The resulting product is denoted as HP-ZIF-61.

Materials characterization

X-ray diffraction (XRD) patterns of the HP-MOF samples were recorded on a diffractometer system (D8 ADVANCE, Bruker AXS) using a Cu sealed tube (40 kV, 40 mA, wavelength $\lambda = 0.15418$ nm) at room temperature and pressure. Fourier transform infrared (FT-IR) spectra of HP-MOFs were recorded on an FT-IR spectrometer (Vector 33, Bruker Corporation) with a resolution of 4 cm^{-1} . Nitrogen (N_2) adsorption-desorption measurements at 77 K were performed on an ASAP 2020 or 2460 (Micromeritics), and all samples were outgassed for overnight at 393 K before measurement to remove the guest molecules trapped in the pores. The morphologies of the samples were characterized by using scanning electron microscope (SEM; ZEISS Ultra 55, Carl Zeiss) at a low loading energy and voltage of 5.0 kV and transmission electron microscopy (TEM, JEM-2100HR, JEOL). Thermogravimetric analysis (TGA) data were obtained using a TG analyzer (TG 209, Tarsus, NETZSCH) and heated from 298 to 873 K in N_2 atmosphere at a rate of 5 K min^{-1} . The CH_4 adsorption curve was obtained on a RUBOTHERM magnetic suspension balance.

Calculation

We applied density functional theory (DFT) method to calculate electrostatic properties of the surfactant so as to investigate the difference between amines and halogenated alkane in the rapid formation process of HP-MOFs [36]. Geometry optimization was performed at the B3LYP level with 6-311+G(d, p) basis set in the Gaussian 09 [37]. The chosen basis set offers the basis functions for a variety range of organic compounds with fair accuracy [38]. The molecular electrostatic potential (MEP) of surfactant molecules was calculated at B3LYP/6-31+G* level.

Calculation of STY

Space-time yield (STY) is an important parameter for the industrial production of the product [33] and can be calculated by Eq. (1)

$$\text{STY} = \frac{m_{\text{MOF}}}{V_{\text{solution}} \cdot \tau} \times 1.44 \times 10^6 \quad (1)$$

where m_{MOF} represents the powder mass (g) of the HP-MOFs, V_{solution} represents the total volume (cm^3) of the mixture, and τ represents the reaction time (min).

Results and discussion

Figure 1a shows the wide-angle XRD patterns of the HP-Cu-BTC sample synthesized with a cooperative template method and the C-Cu-BTC, as well as the

simulated XRD pattern of Cu-BTC single-crystal. It can be clearly observed from Fig. 1a that the XRD patterns of the as-synthesized HP-Cu-BTC are consistent with those of C-Cu-BTC and the simulated Cu-BTC, indicating that the obtained product is topologically identical to Cu-BTC crystal [29]. Moreover, the sharp XRD peaks of HP-Cu-BTC confirm fine crystallinity [37]. The crystal structure of HP-Cu-BTC was further characterized using FT-IR spectroscopy. As shown in Fig. 1b, the FT-IR spectra of HP-Cu-BTC reveal that the carboxylate group $\nu(\text{OCO})$ of ligand (H_3BTC) was coordinated to metal ions (Cu^{2+}) [39]. The absorption bands of HP-Cu-BTC at ca. 1560, 1450 and $\sim 1370 \text{ cm}^{-1}$ were clearly identified as pure Cu-BTC [40], verifying again that the obtained product is crystalline Cu-BTC. Furthermore, the characteristic C-N stretching vibration of template at around $1230\text{--}1030 \text{ cm}^{-1}$ was not observed, confirming that HP-Cu-BTC is free of template, which can be attributed to the introduced template was removed easily by the treatment of activation and drying [41]. Therefore, the FT-IR results indicate the coordination between Cu^{2+} and ligand (H_3BTC) in the framework.

The porosities of the attained samples were measured by N_2 adsorption–desorption method after all samples were treated. As shown in Fig. 2a, the N_2 adsorption–desorption isotherms of C-Cu-BTC exhibit a type I mode with a sharp increased uptake at the initial stage followed by a flatland, which is a characteristic of microporous materials [37]. Nevertheless, the N_2 adsorption–desorption isotherms of

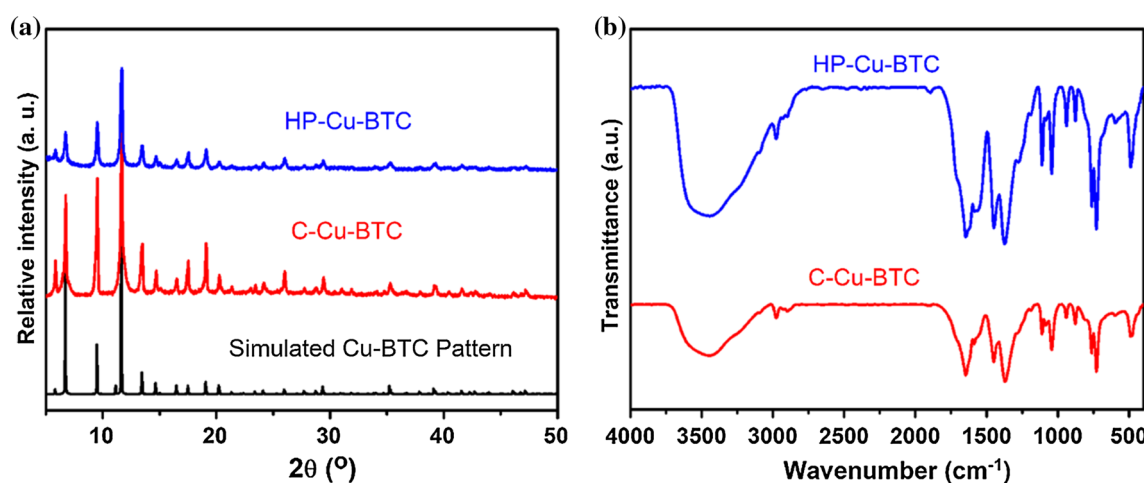


Figure 1 **a** Powder XRD patterns of HP-Cu-BTC, C-Cu-BTC and the simulated Cu-BTC pattern; **b** FT-IR spectra of HP-Cu-BTC and C-Cu-BTC samples.

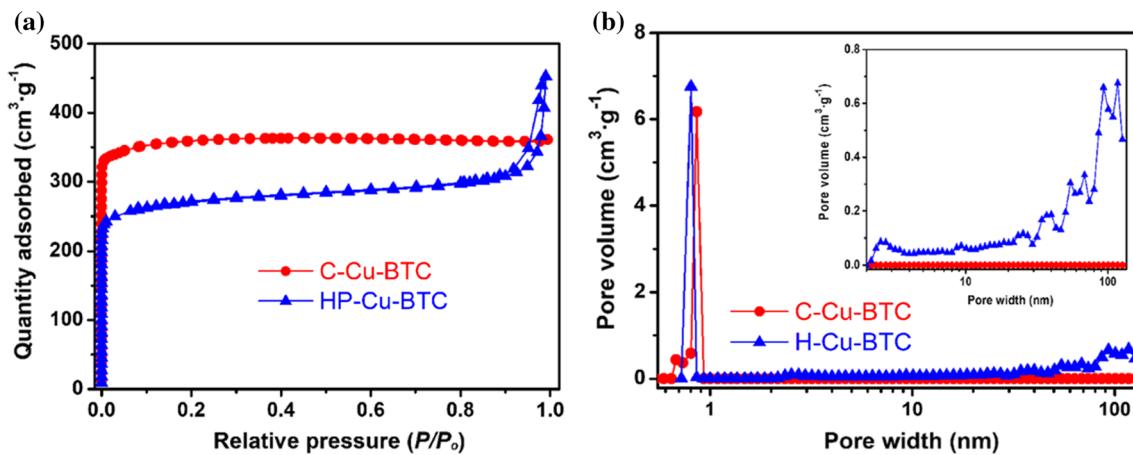


Figure 2 **a** The N₂ adsorption–desorption isotherms and **b** pore size distributions of HP–Cu–BTC and C–Cu–BTC samples.

the HP–Cu–BTC show an intermediate mode between type I and type IV with a high N₂ uptake at low relative pressure region of $P/P_0 < 0.01$, indicating the presence of abundant micropores [32]. Moreover, a large type-H4 hysteresis loop can be observed at high relative pressure ($P/P_0 > 0.8$), related to capillary condensation of N₂ in mesopores [42], confirming the formation of mesopores in HP–Cu–BTC sample, similar behavior has been observed in a previous report [18, 43]. In addition, it should be pointed out that the adsorption capacity of HP–Cu–BTC is inferior to that of C–Cu–BTC at low relative pressure ($P/P_0 < 0.01$), which can be attributed to the HP–Cu–BTC has a lower Brunauer–Emmett–Teller (BET) surface area than that of C–Cu–BTC [44].

More detail regarding the porosity properties of these samples can be gained from the pore size distributions (calculated from nonlocal density functional theory (NL-DFT) analysis). As shown in Fig. 2b, the C–Cu–BTC only possesses micropores with pore size distribution centered at around 0.86 nm, which is consistent with previous report [34]. However, for the HP–Cu–BTC sample, other than the intrinsic micropores, it contains a broad pore size distribution from 30 to over 100 nm (inset of Fig. 2b), including mesoporous and macroporous regions. These analyses confirm that the as-synthesized HP–Cu–BTC product possesses hierarchical pores with micropores, mesopores and macropores. As shown in Table 1, the attained HP–Cu–BTC shows a lower Brunauer–Emmett–Teller (BET) surface areas ($S_{\text{BET}} = 907 \text{ m}^2 \text{ g}^{-1}$) than those of the C–Cu–BTC ($S_{\text{BET}} = 1425 \text{ m}^2 \text{ g}^{-1}$) and previously reported Cu–BTC [33], as confirmed by the N₂ adsorption–

desorption isotherms (Fig. 2a). The lower S_{BET} can be ascribed to the pore impenetration [45]. However, HP–Cu–BTC has a much larger mesopore volume ($V_{\text{meso}} = 0.24 \text{ cm}^3 \text{ g}^{-1}$) and the mesopore surface area (S_{meso}) to micropore surface area (S_{micro}) ($S_{\text{meso}}/S_{\text{micro}} = 0.25$) than that of C–Cu–BTC ($V_{\text{meso}} = 0.06 \text{ cm}^3 \text{ g}^{-1}$, $S_{\text{meso}}/S_{\text{micro}} = 0.09$), respectively. These results further verify the formation of mesoporosity in the HP–Cu–BTC.

SEM and TEM were applied to track the morphology and particle size of product [46, 47]. As illustrated in Fig. 3a, the as-synthesized C–Cu–BTC crystal exhibits a typical octahedron in shape with crystal dimension about 10 μm. Moreover, smooth surfaces can be clearly observed from the Fig. 3a–c, respectively, consistent with previous reports [34]. However, HP–Cu–BTC consists of nanoparticles with particle size of 500 nm (Fig. 3b). The smaller crystals in HP–Cu–BTC can be attributed to the rapid growth of frameworks [33, 48]. In addition, the high-dispersive nanoparticles are randomly stacked together and form abundant pore voids, as shown in Fig. 3b–d, respectively. Similar to previously reported that hierarchical pores were formed through the aggregation or packing of nanoparticles [49, 50]. Moreover, the scan mapping shows that the presence of elemental C, O and Cu with uniform distribution in the HP-MOF particles (Fig. S1) further verifies the chemical composition of the crystal [32]. Excellent stability of materials is necessary for the practical applications [51]. Therefore, the thermal stability of the as-synthesized HP-MOFs was investigated by TGA under a N₂ atmosphere. As shown in Fig. S2, the TGA curve of HP–Cu–BTC indicates that the product

Table 1 Textural properties of HP-MOFs and C-Cu-BTC samples

Sample	S_{BET}^a ($\text{m}^2 \text{ g}^{-1}$)	S_{micro}^b ($\text{m}^2 \text{ g}^{-1}$)	$S_{\text{meso}}/S_{\text{micro}}^c$	V_t^d ($\text{cm}^3 \text{ g}^{-1}$)	V_{meso}^e ($\text{cm}^3 \text{ g}^{-1}$)	V_{micro}^f ($\text{cm}^3 \text{ g}^{-1}$)
C–Cu–BTC	1425	1308	0.09	0.56	0.06	0.50
HP–Cu–BTC	907	727	0.25	0.57	0.24	0.32
HP–Cu–BTC_A	1099	904	0.22	0.59	0.17	0.42
HP–Cu–BTC_B	1123	897	0.25	0.92	0.50	0.42

^a S_{BET} Brunauer–Emmett–Teller (BET) surface area

^b S_{micro} micropore surface area

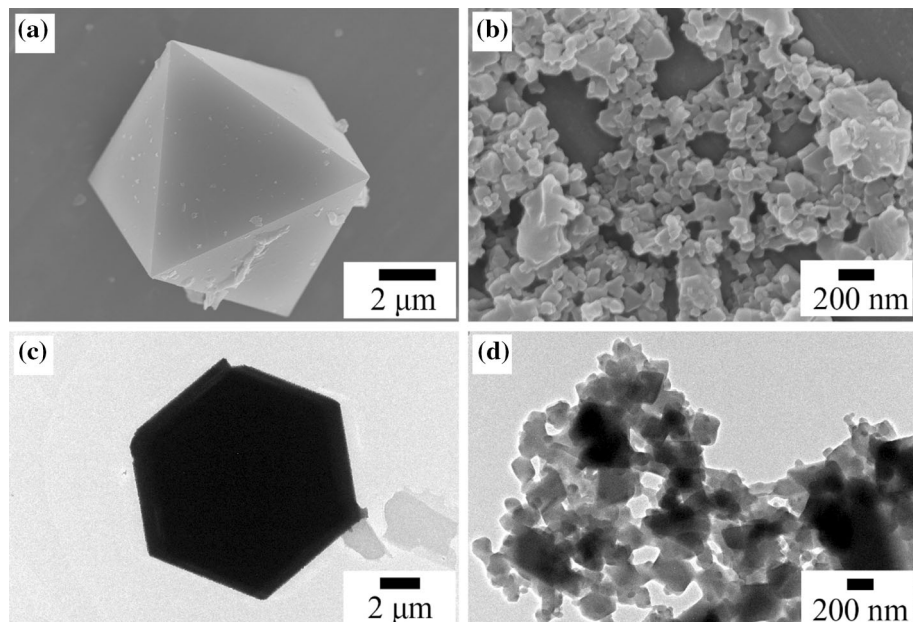
^c S_{meso} mesopore surface area

^d V_t total pore volume

^e V_{meso} mesopore volume

^f V_{micro} micropore volume

Figure 3 SEM and TEM images of **a**, **c** C–Cu–BTC and **b**, **d** HP–Cu–BTC samples.



undergoes three stages of weight loss; in the initial stage of weight loss occurred at 90 °C corresponding to the removal of trapped guest molecules (e.g., H₂O) [52]. The second stage of weight loss which takes place at approximately 150 °C may be ascribed to the evaporation of template and DMF [53]. Subsequently, the TGA curve of HP–Cu–BTC exhibits a drop sharply after 320 °C, corresponding to the decomposition of framework [29]. By comparison, the collapse temperature of the sample HP–Cu–BTC (320 °C) is similar to that of C–Cu–BTC (320 °C) during the same thermal treatment, indicating that the introduction of mesopores and macropores does not degrade the thermal stability of the HP-MOFs [32].

In our previous study, amine surfactant (e.g., DOE) could be used as structure-directing agents (SDAs) to prepare HP-MOFs such as Cu–BTC and ZIF-8 under hydrothermal conditions, indicating the introduced DOE played a role of template during the synthesis [18]. Additionally, the Tyndall scattering effect appeared in the colloidal suspension of DOE indicated that the supramolecular micelles were formed through self-assembly [54], as shown in Fig. S3. However, in our most recent work, the selected halogenated alkenes such as 1-bromohexadecane cannot individually act as template to prepare HP-MOFs under same synthesis conditions owing to its weak interactions with ligands [32]. In order to

explore the difference between the amine and halogenated alkane for the rapid formation process of HP-MOFs, theoretical calculation was applied to study the molecular property of surfactants. The optimized molecular geometries of two surfactants (DOE and 1-bromohexadecane) are demonstrated in Fig. S4. Figure 4 shows the molecular electrostatic potential (MEP) maps of the two surfactants, where the negative regions (red) of MEP maps relate to electrophilic reactivity and the positive regions (blue) to nucleophilic reactivity [29]. The negative regions (red) of the two surfactant molecules are mainly located on the amine and bromine groups, respectively, which indicates the most susceptible sites for electrophilic attacks [55]. The electrostatic potential of DOE located at amine group is lower than bromine group of 1-bromohexadecane, suggesting stronger electrophilic affinity of amines [56]. These theoretical calculations may explain the experimental results that the amines can be applied as template instead of halogenated alkane.

Based on the above experiments and theoretical calculations, a feasible mechanism for the usage of amine surfactant and ZnO to rapidly synthesize HP-MOFs is proposed and illustrated in Scheme 1. During the synthesis system, on the one hand, the introduced DOE forms supramolecular micelles through self-assembly in the ligand solution, and then the micelles surrounded by the ligands through an appropriate interaction [57, 58]. On the other hand, the introduced ZnO can react with Cu^{2+} to form (Cu, Zn) HDS (an intermediate that was dissolved completely in solution), which exhibits a high rate of anion exchange in the ligand solution and drives the rapid formation of MOF crystal at room temperature and pressure [33, 59]. Thus, ZnO played the role of an accelerator. Upon the (Cu, Zn) HDS was added to the mixture of the ligand and micelles, the ligand will react with HDS to form MOF frameworks on the surface of micelles [19, 60]. Subsequently,

mesopores and macropores are formed after removing template [19].

For the HP-Cu-BTC_X (X = B and C), as shown in Fig. S5, the XRD patterns and FT-IR spectra of HP-Cu-BTC_X are in close agreement with the simulated Cu-BTC or C-Cu-BTC, respectively, confirming the formation of crystalline Cu-BTC. The N_2 adsorption-desorption isotherms and electron microscopy (SEM and TEM) images demonstrate that the attained HP-Cu-BTC_X possesses hierarchical pores (see Figs. S6–7 in the Supporting Information for details). Moreover, as shown in Table 1, the prepared HP-Cu-BTC_X exhibits high V_{meso} and $S_{\text{meso}}/S_{\text{micro}}$, further confirming the formation of mesopores. Notably, the mesoporosity of HP-MOFs depends on the type of templates (Table 1), which allows us control the porosity of HP-MOFs, such as S_{BET} , V_t and V_{meso} . Furthermore, all HP-Cu-BTC_X samples have excellent thermal stabilities (Fig. S2). More importantly, our synthesis strategy has a highly versatile due to other HP-MOFs such as ZIF-8 and ZIF-61 were also synthesized at room temperature (denoted as HP-ZIF-8 and HP-ZIF-61, respectively, see experiment “Rapid room-temperature synthesis of hierarchically porous ZIF-8” and “Rapid room-temperature synthesis of hierarchically porous ZIF-61” sections). As shown in Fig. S8a, all diffraction peak positions of the HP-ZIF-8 sample well agreed with the simulation result, confirming the product obtained from rapid synthesis is crystalline ZIF-8. The FT-IR spectra of HP-ZIF-8 sample are in agreement with that of conventional ZIF-8 (C-ZIF-8) (Fig. S8b), which is clearly identified as pure ZIF-8 [61]. The N_2 adsorption-desorption isotherms of the HP-ZIF-8 sample show an intermediate mode between type I and type IV (Fig. 5a), which is related to the coexistence of mesopores and micropores [62]. By comparison, the isotherms of C-ZIF-8 exhibit a type I mode (Fig. S9a), which is related to microporous materials [63]. Moreover, we can acquire more information concerning porosity

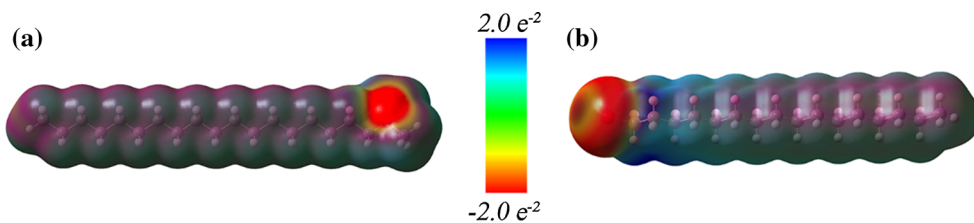
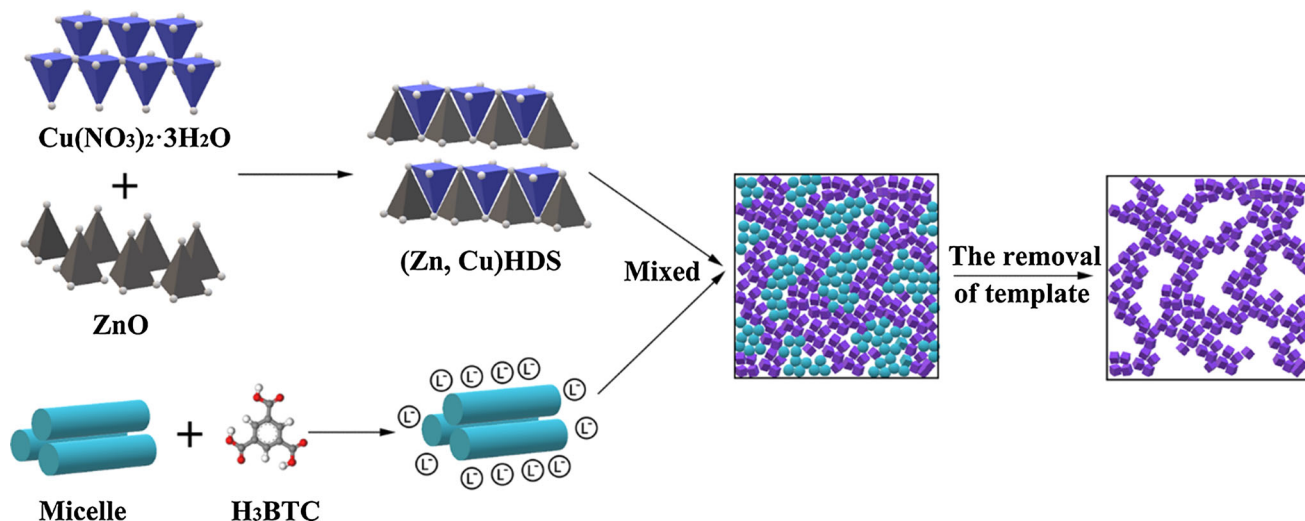


Figure 4 Molecular electrostatic potential (MEP) maps of **a** *N,N*-dimethyloctadecylamine (DOE) and **b** 1-bromohexadecane (hydrogen atoms: white balls, carbon atoms: gray balls, bromine atoms: crimson balls, and nitrogen atoms: blue balls).



Scheme 1 Schematic of the rapid room-temperature synthesis of HP-MOFs by the simultaneous introduction of surfactant and ZnO during the synthesis system.

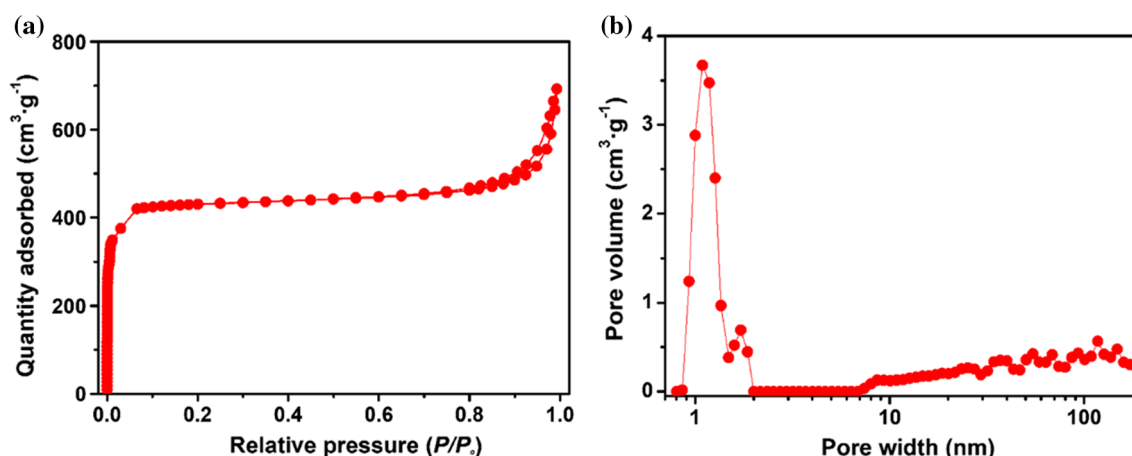


Figure 5 **a** The N_2 adsorption–desorption isotherms and **b** pore size distributions of HP-ZIF-8.

from the pore size distributions [18]. As shown in Fig. 5b, in addition to the intrinsic micropores, HP-ZIF-8 sample also embraces the mesopore and macropore regions, which is absent in the C-ZIF-8 (Fig. S9b). Furthermore, SEM and TEM images (Fig. S10) displayed that HP-ZIF-8 product has an apparent mesovoid phase, which indicates that HP-ZIF-8 possesses mesoporous structures. Moreover, the as-synthesized HP-ZIF-8 exhibits good thermostability (Fig. S11). Similarly, HP-ZIF-61 sample prepared from the rapid synthesis also possesses a hierarchical porous structure (see Figs. S12–13). In addition to organic amines, other surfactants such as *n*-butyl alcohol and lauric acid can also be used as templates to rapidly fabricate HP-MOFs (HP-Cu-BTC_D and HP-Cu-BTC_E) (see Figs. S14–15 in the

Supporting Information for details). These results indicate that our template method developed in this work is well versatile.

The introduction of mesopores and macropores into microporous MOFs can effectively improve adsorption performance of guest molecules [17]. To evaluate the adsorption properties of the HP-ZIF-8, single-component gas such as CH_4 was selected as probe reactant. Figure 6 exhibits the isotherms of CH_4 on HP-ZIF-8 and C-ZIF-8 measured at a broad range of high pressures at 298 K. It can be seen that the adsorption isotherm of CH_4 on the HP-ZIF-8 is always higher than that on C-ZIF-8, implying the former has higher uptake capacities of CH_4 than the latter, *i.e.*, at 3 MPa and 273 K, the CH_4 uptake of HP-ZIF-8 is 68.4 mg/g, having an increase of 63.6%

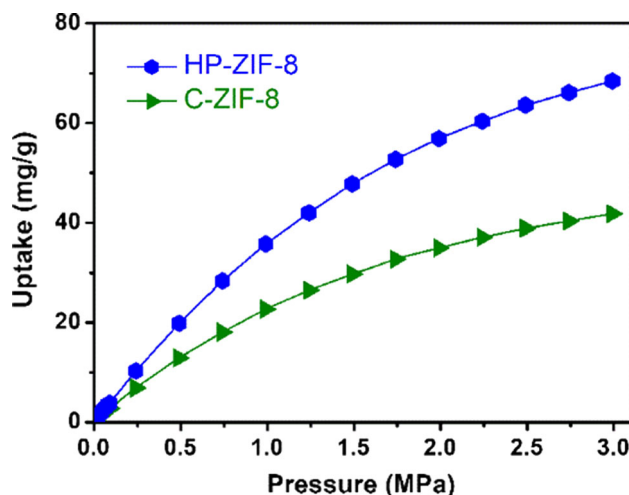


Figure 6 Adsorption curves of CH₄ on HP-ZIF-8 and C-ZIF-8 at 298 K, under pressures up to 3 MPa.

compared to that of C-ZIF-8 (41.8 mg/g). The significantly increase in CH₄ uptake capacity can be attributed not only to an enhancement in the surface area of HP-ZIF-8, but also to the increase in the pore volume [64].

In addition to the porosity properties, energy consumption and production rate are two essential factors for the large-scale preparation of HP-MOFs due to them determine the environmental influence (e.g., carbon footprint) and manufacturing cost [12, 65]. In comparison with conventional template method for synthesizing HP-MOFs requires a long reaction time at high temperature and pressure, our strategy developed in this work realizes the rapid room-temperature synthesis of various HP-MOFs by the simultaneous introduction of surfactant and ZnO, which satisfies with the environmental-friendly and low-cost demands for the production of HP-MOFs. STY of a reaction is essential consideration to assess the viability of scale up, which should be as high as possible [31, 51]. For 11 min reactions, the STY of HP-Cu-BTC is as high as 2575 kg m⁻³ d⁻¹, which is one order of magnitude higher than that of the commercial product Basolite C300 (225 kg m³ per day) [65], and also surpasses the previous report (1123 kg m⁻³ d⁻¹) [32]. A plausible explanation of such high STY of HP-Cu-BTC may be attributed to the reduction in synthesis time [28]. Moreover, the STY of HP-Cu-BTC synthesized with tonne scale ($> 1 \times 10^3$ kg m⁻³ d⁻¹) is comparable to that of an Al-MOFs with large-scale production [66]. Therefore, our synthesis strategy may open up a pathway for the

commercialized preparation of HP-MOFs which by means of conventional hydrothermal methods were not accessible on an industrial level before.

Conclusions

In summary, three stable HP-MOFs (Cu-BTC, ZIF-8 and ZIF-61) have been prepared using a simple and straightforward room-temperature synthesis strategy. Specifically, the synthesis conditions have been optimized, which can shorten the synthesis time to 11 min. Additionally, the obtained products exhibited multimodal hierarchical porous structures with micropores, mesopores and macropores. The STY of the produced HP-Cu-BTC is up to 2575 kg m⁻³ d⁻¹, which is much higher than previously reported (1123 kg m⁻³ d⁻¹). Moreover, theoretical calculations have illustrated the differences in surfactant type for the rapid formation of HP-MOFs. Consequently, a novel synthesis mechanism is proposed. The resulting HP-MOFs have much higher gas uptake capacity than that of conventional MOFs. Among them, the maximum CH₄ uptake of HP-MOFs is 68.4 mg/g, which is 63.6% higher than that of microporous MOFs. Importantly, our synthesis strategy has a versatility due to other surfactants can also be used as templates, while other HP-MOFs can also be synthesized rapidly under mild synthesis conditions. The method developed in this work represents a versatile industrial method for the large-scale production of a wide variety of HP-MOFs.

Acknowledgements

We gratefully acknowledge the financial support from the National Natural Science Foundation of China (No. 21576094), SRFDP (No. 20130172110012) and Guangdong Natural Science Foundation (2017A030313052).

Compliance with ethical standards

Conflicts of interest There are no conflicts to declare.

Electronic supplementary material: The online version of this article (<https://doi.org/10.1007/s108>

53-018-2793-3) contains supplementary material, which is available to authorized users.

References

- [1] Yang Q, Xu Q, Jiang H-L (2017) Metal–organic frameworks meet metal nanoparticles: synergistic effect for enhanced catalysis. *Chem Soc Rev* 46:4774. <https://doi.org/10.1039/C6CS00724D>
- [2] Dolgopolova EA, Rice AM, Martin CR, Shustova NB (2018) Photochemistry and photophysics of MOFs: steps towards MOF-based sensing enhancements. *Chem Soc Rev*. <https://doi.org/10.1039/C7CS00861A>
- [3] Wang H, Lustig WP, Li J (2018) Sensing and capture of toxic and hazardous gases and vapors by metal–organic frameworks. *Chem Soc Rev*. <https://doi.org/10.1039/C7CS00885F>
- [4] Zheng B, Huang L, Cao X et al (2018) A highly porous acylamide decorated MOF-505 analogue exhibiting high and selective CO₂ gas uptake capability. *CrystEngComm* 20:1874. <https://doi.org/10.1039/C8CE00103K>
- [5] Qian X, Ren Q, Wu X, Sun J, Wu H, Lei J (2018) Enhanced water stability in Zn-doped zeolitic imidazolate Framework-67 (ZIF-67) for CO₂ Capture Applications. *ChemistrySelect* 3:657. <https://doi.org/10.1002/slct.201702114>
- [6] Zhao Y, Liu J, Horn M, Motta N, Hu M, Li Y (2018) Recent advancements in metal organic framework based electrodes for supercapacitors. *Sci China Mater* 61:159. <https://doi.org/10.1007/s40843-017-9153-x>
- [7] Gao X, Wang Y, Ji G, Cui R, Liu Z (2018) One-pot synthesis of hierarchical-pore metal–organic frameworks for drug delivery and fluorescent imaging. *CrystEngComm* 20:1087. <https://doi.org/10.1039/C7CE02053H>
- [8] Yang Y, Liu X, Yan D, Deng P, Guo Z, Zhan H (2018) Europium ion post-functionalized zirconium metal–organic frameworks as luminescent probes for effectively sensing hydrazine hydrate. *RSC Adv* 8:17471. <https://doi.org/10.1039/C8RA03049A>
- [9] Tian P, He X, Li W et al (2018) Zr-MOFs based on Keggin-type polyoxometalates for photocatalytic hydrogen production. *J Mater Sci*. <https://doi.org/10.1007/s10853-018-2476-0>
- [10] Ma L, Abney C, Lin W (2009) Enantioselective catalysis with homochiral metal–organic frameworks. *Chem Soc Rev* 38:1248. <https://doi.org/10.1039/B807083K>
- [11] Lin S, Bediako JK, Cho C-W et al (2018) Selective adsorption of Pd(II) over interfering metal ions (Co(II), Ni(II), Pt(IV)) from acidic aqueous phase by metal–organic frameworks. *Chem Eng J* 345:337. <https://doi.org/10.1016/j.cej.2018.03.173>
- [12] Julien PA, Mottillo C, Friscic T (2017) Metal–organic frameworks meet scalable and sustainable synthesis. *Green Chem* 19:2729. <https://doi.org/10.1039/C7GC01078H>
- [13] Yin W, C-a Tao F, Wang J Huang, Qu T, Wang J (2018) Tuning optical properties of MOF-based thin films by changing the ligands of MOFs. *Sci China Mater* 61:391. <https://doi.org/10.1007/s40843-017-9143-5>
- [14] Kayal S, Chakraborty A (2018) Activated carbon (type Maxsorb-III) and MIL-101(Cr) metal organic framework based composite adsorbent for higher CH₄ storage and CO₂ capture. *Chem Eng J* 334:780. <https://doi.org/10.1016/j.cej.2017.10.080>
- [15] Szuromi P (2018) Mesoporous metal–organic frameworks. *Science* 359:172. <https://doi.org/10.1126/science.359.6372.172-i>
- [16] Ma S, Sun D, Simmons JM, Collier CD, Yuan D, Zhou H-C (2008) Metal–organic framework from an anthracene derivative containing nanoscopic cages exhibiting high methane uptake. *J Am Chem Soc* 130:1012. <https://doi.org/10.1021/ja0771639>
- [17] Gu X, Lu Z-H, Xu Q (2010) High-connected mesoporous metal–organic framework. *Chem Commun* 46:7400. <https://doi.org/10.1039/C0CC02808H>
- [18] Duan C, Li F, Zhang H, Li J, Wang X, Xi H (2017) Template synthesis of hierarchical porous metal–organic frameworks with tunable porosity. *RSC Adv* 7:52245. <https://doi.org/10.1039/C7RA08798E>
- [19] Qiu LG, Xu T, Li ZQ et al (2008) Hierarchically micro- and mesoporous metal–organic frameworks with tunable porosity. *Angew Chem* 47:9487. <https://doi.org/10.1002/anie.200803640>
- [20] Xueqing Y, Wei C, Haidong B et al (2018) Synthesis of mesoporous ZIF-8 nanoribbons and their conversion into carbon nanoribbons for high-performance supercapacitors. *Chem Eur J*. <https://doi.org/10.1002/chem.201801869>
- [21] Kim Y, Yang T, Yun G et al (2015) Hydrolytic transformation of microporous metal–organic frameworks to hierarchical micro-and mesoporous MOFs. *Angew Chem Int Edit* 54:13273
- [22] Zhao Y, Zhang J, Han B, Song J, Li J, Wang Q (2011) metal–organic framework nanospheres with well-ordered mesopores synthesized in an ionic liquid/CO₂/surfactant system. *Angew Chem Int Edit* 50:636
- [23] Cai G, Jiang H-L (2017) A modulator-induced defect-formation strategy to hierarchically porous metal–organic frameworks with high stability. *Angew Chem Int Edit* 56:563. <https://doi.org/10.1002/anie.201610914>
- [24] Carne-Sanchez A, Imaz I, Cano-Sarabia M, Maspoch D (2013) A spray-drying strategy for synthesis of nanoscale metal–organic frameworks and their assembly into hollow

- superstructures. *Nat Chem* 5:203. <https://doi.org/10.1038/nchem.1569>
- [25] Chou L-Y, Hu P, Zhuang J et al (2015) Formation of hollow and mesoporous structures in single-crystalline microcrystals of metal–organic frameworks via double-solvent mediated overgrowth. *Nanoscale* 7:19408. <https://doi.org/10.1039/c5nr06532a>
- [26] He X, Yang C, Wang D, Gilliland Iii SE, Chen D-R, Wang W-N (2017) Facile synthesis of ZnO@ZIF core-shell nanofibers: crystal growth and gas adsorption. *CrystEngComm* 19:2445. <https://doi.org/10.1039/C7CE00368D>
- [27] Chen Y, Ni D, Yang X, Liu C, Yin J, Cai K (2018) Microwave-assisted synthesis of honeycomblike hierarchical spherical Zn-doped Ni-MOF as a high-performance battery-type supercapacitor electrode material. *Electrochim Acta* 278:114. <https://doi.org/10.1016/j.electacta.2018.05.024>
- [28] Stock N, Biswas S (2012) Synthesis of metal–organic frameworks (MOFs): routes to various MOF topologies, morphologies, and composites. *Chem Rev* 112:933. <https://doi.org/10.1021/cr200304e>
- [29] Duan C, Li F, Luo S, Xiao J, Li L, Xi H (2018) Facile synthesis of hierarchical porous metal–organic frameworks with enhanced catalytic activity. *Chem Eng J* 334:1477. <https://doi.org/10.1016/j.cej.2017.11.086>
- [30] Fu Z, Chuan-Ling Z, Huang-Yong P, Huai-Ping C, Hai-Sheng Q (2016) Near-infrared photocatalytic upconversion nanoparticles/TiO₂ nanofibers assembled in large scale by electrospinning. *Part Part Syst Char* 33:248. <https://doi.org/10.1002/ppsc.201600010>
- [31] Huo J, Brightwell M, El Hankari S, Garai A, Bradshaw D (2013) Industrially relevant, aqueous room temperature synthesis of HKUST-1 with high space–time yield. *J Mater Chem A* 1:15220. <https://doi.org/10.1039/C3TA14409G>
- [32] Duan C, Li F, Li L et al (2018) Hierarchically structured metal–organic frameworks assembled by hydroxy double salt-template synergy with high space–time yields. *CrystEngComm* 20:1057. <https://doi.org/10.1039/C7CE01843F>
- [33] Zhao J, Nunn WT, Lemaire PC et al (2015) Facile conversion of hydroxy double salts to metal–organic frameworks using metal oxide particles and atomic layer deposition thin-film templates. *J Am Chem Soc* 137:13756. <https://doi.org/10.1021/jacs.5b08752>
- [34] Chui SS-Y, Lo SM-F, Charmant JP, Orpen AG, Williams ID (1999) A chemically functionalizable nanoporous material [Cu₃(TMA)₂(H₂O)₃] n. *Science* 283:1148
- [35] Li Z, Huang X, Sun C, Chen X, Hu J, Stein A, Tang B (2017) Thin-film electrode based on zeolitic imidazolate frameworks (ZIF-8 and ZIF-67) with ultra-stable performance as a lithium-ion battery anode. *J Mater Sci* 52:3979. <https://doi.org/10.1007/s10853-016-0660-7>
- [36] Singha Deb AK, Dwivedi V, Dasgupta K, Musharaf Ali S, Shenoy KT (2017) Novel amidoamine functionalized multi-walled carbon nanotubes for removal of mercury(II) ions from wastewater: combined experimental and density functional theoretical approach. *Chem Eng J* 313:899. <https://doi.org/10.1016/j.cej.2016.10.126>
- [37] Chongxiong D, Hang Z, Anguo P et al (2018) Synthesis of hierarchically structured metal–organic frameworks by a dual-functional surfactant. *ChemistrySelect* 3:5313. <https://doi.org/10.1002/slct.201800571>
- [38] Duan C, Li F, Xiao J, Liu Z, Li C, Xi H (2017) Rapid room-temperature synthesis of hierarchical porous zeolitic imidazolate frameworks with high space–time yield. *Sci China Mater* 60:1205. <https://doi.org/10.1007/s40843-017-9136-y>
- [39] Zhu C, Zhang Z, Wang B et al (2016) Synthesis of HKUST-1#MCF compositing materials for CO₂ adsorption. *Micropor Mesopor Mat* 226:476. <https://doi.org/10.1016/j.micromeso.2016.02.029>
- [40] Kim S-Y, Kim A-R, Yoon JW, Kim H-J, Bae Y-S (2018) Creation of mesoporous defects in a microporous metal–organic framework by an acetic acid-fragmented linker co-assembly and its remarkable effects on methane uptake. *Chem Eng J* 335:94. <https://doi.org/10.1016/j.cej.2017.10.078>
- [41] Bradshaw D, El-Hankari S, Lupica-Spagnolo L (2014) Supramolecular templating of hierarchically porous metal–organic frameworks. *Chem Soc Rev* 43:5431
- [42] Shi Z, Li L, Xiao Y et al (2017) Synthesis of mixed-ligand Cu–MOFs and their adsorption of malachite green. *RSC Adv* 7:30904. <https://doi.org/10.1039/C7RA04820C>
- [43] Sun L-B, Li J-R, Park J, Zhou H-C (2011) Cooperative template-directed assembly of mesoporous metal–organic frameworks. *J Am Chem Soc* 134:126
- [44] Gregg SJ, Sing KSW, Salzberg H (1967) Adsorption surface area and porosity. *J Electrochem Soc* 114:279C
- [45] Peng L, Zhang J, Xue Z et al (2014) Highly mesoporous metal–organic framework assembled in a switchable solvent. *Nat Commun* 5:4465. <https://doi.org/10.1038/ncomms5465>
- [46] Wang Z, Hu S, Yang J et al (2018) Nanoscale Zr based MOFs with tailororable size and introduced mesopore for protein delivery. *Adv Funct Mater*. <https://doi.org/10.1002/adfm.201707356>
- [47] Wang X, Zhan C, Ding Y et al (2017) Dual-core Fe₂O₃@-Carbon structure derived from hydrothermal carbonization of chitosan as a highly efficient material for selective adsorption. *ACS Sustain Chem Eng* 5:1457. <https://doi.org/10.1021/acssuschemeng.6b02034>
- [48] Gross AF, Sherman E, Vajo JJ (2012) Aqueous room temperature synthesis of cobalt and zinc sodalite zeolitic

- imidizolate frameworks. *Dalton T* 41:5458. <https://doi.org/10.1039/C2DT30174A>
- [49] Cao Y, Ma Y, Wang T, Wang X, Huo Q, Liu Y (2016) Facile fabricating hierarchically porous metal–organic frameworks via a template-free strategy. *Cryst Growth Des* 16:504. <https://doi.org/10.1021/acs.cgd.5b01559>
- [50] Hirai K, Furukawa S, Kondo M, Uehara H, Sakata O, Kitagawa S (2011) Sequential functionalization of porous coordination polymer crystals. *Angew Chem Int Edit* 50:8057. <https://doi.org/10.1002/anie.201101924>
- [51] Bian C, Zhang C, Pan S et al (2017) Generalized high-temperature synthesis of zeolite catalysts with unpredictably high space–time yields (STYs). *J Mater Chem A* 5:2613. <https://doi.org/10.1039/C6TA09866E>
- [52] Cravillon J, Münzer S, Lohmeier S-J, Feldhoff A, Huber K, Wiebcke M (2009) Rapid room-temperature synthesis and characterization of nanocrystals of a prototypical zeolitic imidazolate framework. *Chem Mater* 21:1410
- [53] Aarti S Bhadauria, Nanoti A et al (2016) $[\text{Cu}_3(\text{BTC})_2]$ -polyethyleneimine: an efficient MOF composite for effective CO_2 separation. *RSC Adv* 6:93003. <https://doi.org/10.1039/C6RA10465G>
- [54] Singh A, Ojha AK, Jang HM (2018) Strategic design and utilization of molecular flexibility for straddling the application of organic superbases: a DFT Study. *ChemistrySelect* 3:837. <https://doi.org/10.1002/slct.201702912>
- [55] Wan Y, Zhao D (2007) On the controllable soft-templating approach to mesoporous silicates. *Chem Rev* 107:2821
- [56] Roy DR, Parthasarathi R, Padmanabhan J, Sarkar U, Subramanian V, Chattaraj PK (2006) Careful scrutiny of the philicity concept. *J Phys Chem A* 110:1084. <https://doi.org/10.1021/jp053641v>
- [57] Wan Y, Shi Y, Zhao D (2008) Supramolecular aggregates as templates: ordered mesoporous polymers and carbons. *Chem Mater* 20:932. <https://doi.org/10.1021/cm7024125>
- [58] Moliner M, Rey F, Corma A (2013) Towards the rational design of efficient organic structure-directing agents for zeolite synthesis. *Angew Chem Int Edit* 52:13880. <https://doi.org/10.1002/anie.201304713>
- [59] Zhao J, Kalanyan B, Barton HF, Sperling BA, Parsons GN (2017) In situ time-resolved attenuated total reflectance infrared spectroscopy for probing metal–organic framework thin film growth. *Chem Mater* 29:8804. <https://doi.org/10.1021/acs.chemmater.7b03096>
- [60] Meyn M, Beneke K, Lagaly G (1993) Anion-exchange reactions of hydroxy double salts. *Inorg Chem* 32:1209
- [61] Wang X, Liu J, Leong S et al (2016) Rapid construction of $\text{ZnO}@\text{ZIF}-8$ heterostructures with size-selective photocatalysis properties. *ACS Appl Mater Inter* 8:9080. <https://doi.org/10.1021/acsami.6b00028>
- [62] Yang X, Wu S, Wang P, Yang L (2018) Hierarchical 3D ordered meso-/macroporous metal–organic framework produced through a facile template-free self-assembly. *J Solid State Chem* 258:220. <https://doi.org/10.1016/j.jssc.2017.10.020>
- [63] Xukun Q, Qingbao R, Xiaofei W, Jing S, Hongyu W, Jun L (2018) Enhanced water stability in Zn-doped zeolitic imidazolate framework-67 (ZIF-67) for CO_2 capture applications. *ChemistrySelect* 3:657. <https://doi.org/10.1002/slct.201702114>
- [64] Furukawa H, Ko N, Go YB et al (2010) Ultrahigh Porosity in metal–organic frameworks. *Science* 329:424. <https://doi.org/10.1126/science.1192160>
- [65] Czaja AU, Trukhan N, Muller U (2009) Industrial applications of metal–organic frameworks. *Chem Soc Rev* 38:1284. <https://doi.org/10.1039/B804680H>
- [66] Gaab M, Trukhan N, Maurer S, Gummaraju R, Müller U (2012) The progression of Al-based metal–organic frameworks—from academic research to industrial production and applications. *Micropor Mesopor Mat* 157:131. <https://doi.org/10.1016/j.micromeso.2011.08.016>